RSC Advances

ROYAL SOCIETY OF CHEMISTRY

www.rsc.org/advances

Graphical Abstract

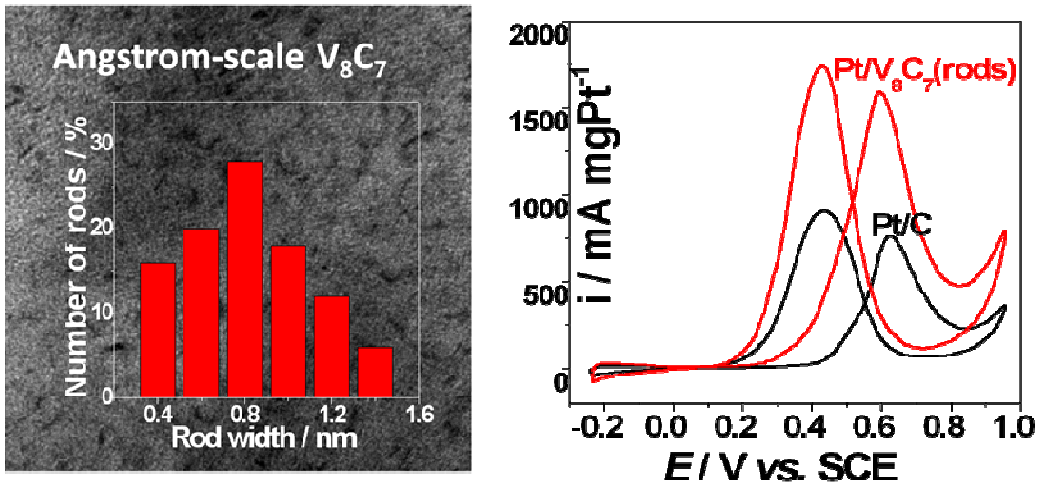

Angstrom-scale vanadium carbide rods as Pt electrocatalyst support for efficient methanol oxidation reaction

Zaoxue Yan*, Lina Gao, Mingmei Zhang, Jimin Xie*, Min Chen

School of Chemistry and Chemical Engineering, Jiangsu University, Zhenjiang, 212013, PR China;

*Corresponding authors. Tel.: +86 11 88791708; Fax: +86 11 88791800. E-mail: yanzaoxue@163.com (Z. Yan); xiejm391@sohu.com (J. Xie).

Abstract

Angstrom-scale vanadium carbide rods combined with carbon (denoted as C-V_8C_7(rods)) are synthesized through an ion-exchange route. The angstrom-scale C-V_8C_7(rods) show better promotion effect on Pt than the nanoscale C-V_8C_7(particles) towards methanol oxidation reaction (MOR). Furthermore, Pt particles loading on C-V_8C_7(rods) (denoted as Pt/C-V_8C_7(rods)) show much higher MOR activity and stability than commercial Pt/C electrocatalyst. The present method is imagined to be adopted to easily synthesize other angstrom-scale materials.

Keywords: Angstrom scale; Vanadium carbide; Pt electrocatalyst; Methanol oxidation reaction; Promotion effect

1. Introduction

Transition metal carbides are efficient as promoters to improve the performances of noble metal based electrocatalysts due to synergistic effect.[1-4] By introducing carbides, the use level of noble metal can be greatly reduced to achieve the same or higher activity.[5-12] Literatures indicated that the interaction between carbide and noble metal increases with the decrease of carbide particle size.[13-15] The larger carbide particles have lower specific surface area, resulting in poor dispersion of loaded noble metal nanoparticles. It is imagined that the mixing of carbide and noble metal at atomic level would lead to full interaction.

The carbides that have been most extensively studied as electrocatalyst promoter are tungsten carbide (WC)[16-23] and molybdenum carbides (MoC and Mo_2C)[24-28]. The recent study indicated that vanadium carbide is more efficient[29] in promoting the activity of platinum (Pt) than WC and Mo_2C, which might make vanadium carbide a new research focus as catalyst promoter. However, the traditional synthesis methods of vanadium carbide (and also other carbides) lead to large particle sizes that are tens or hundreds of nanometers in diameter.[30,31] Recently, in situ exchange routes to vanadium carbide with the diameter down to 2-10 nm[32-35] have been reported, great promotion effects of V_8C_7 on activities of Pt or Pd have been found.

Herein, we report a synthesis of angstrom-scale V_8C_7 with rod-shape. To the best of our knowledge, this is the first attempt to prepare such small V_8C_7 material. It is also

found that Pt being loaded on the synthesized angstrom-scale V_8C_7 rods show excellent activity and stability towards MOR in acidic media.

2. Experimental

2.1 Synthesis of C-V_8C_7 composites

Typically, polyacrylic weak-base anion-exchange resin (10 g, D201×1 resin, Hebi Power Resin Factory, China) was impregnated in 100 ml sodium orthovanadate (SOV, $Na_3VO_4{\cdot}12H_2O$, A.R., Shanghai Ekear Biological Technology Co., Ltd., China) for 6 h, then the solid was separated and dried at 80 ^oC and heated at 800 ^oC for 1 h. After cooled down to room temperature, the sample was ground into powder to get the C-V_8C_7 composite. The samples with SOV concentrations of 0.02 and 0.002 mol L^{-1} were denoted as C-V_8C_7(particles) and C-V_8C_7 (rods) respectively.

2.2 Preparation of electrocatalysts

Pt particles were loaded on the C-V_8C_7 to form Pt/C-V_8C_7 electrocatalyst. Typically, C-V_8C_7 (60 mg) was added into a mixture of 20 ml glycol (A.R., Tianjin Fuyu Fine Chemicals Co., Ltd, China) and chloroplatinic acid (H_2PtCl_6, containing 40 mg Pt, A. R., Sinopharm Chemical Reagent Co., Ltd) and dispersed to form a uniform ink in ultrasonic bath for 30 min. The pH of the mixture was adjusted to 10 by adding 1 mol L^{-1} NaOH/glycol solution. The sample was then put into a microwave oven (900 W) for heating at a 10 s on and 10 s off procedure for 12 times.[36] Afterwards, the mixture was washed with deionized water and dried in vacuum at 50 ^oC for 24 h to get the

Pt/C-V_8C_7 electrocatalyst. The Pt particles being loaded on C-V_8C_7(particles) and C-V_8C_7(rods) were denoted as Pt/C-V_8C_7(particles) and Pt/C-V_8C_7(rods), respectively. The Pt contents in the electrocatalysts were 40 wt% stoichiometricly.

2.3 Preparation of electrodes

Pt/C-V_8C_7 (5 mg) or commercial Pt/C (4 mg, 47.6 wt % Pt, TKK, Japan) were dispersed in mixture of 0.05 ml 5 wt% Nafion suspension (DuPont, USA) and 1.95 ml ethanol in ultrasonic bath to form the electrocatalyst ink. The ink (0.005 ml) was deposited on surface of a glass carbon electrode (0.25 cm^2) and dried at room temperature. The total Pt loadings were 0.02 mg cm^{-2}.

2.4 Electrochemical characterization

All electrochemical measurements were performed in a three-electrode cell on a potentiostat at 30 ^oC. A platinum foil (1.0 cm^2) and saturated calomel electrode (SCE) were used as counter and reference electrodes, respectively. All chemicals were of analytical grade and used as received.

2.5 Physical characterization

The morphologies of the synthesized materials were characterized by transmission electron microscopy (TEM, JOEP JEM-2010, JEOL Ltd.) operating at 200 kV. The structures of the samples were determined on an X-ray diffractometer (XRD, D/Max-IIIA, RigakuCo., Japan,CuK1, λ=1.54056 Å radiation).

3. Results and discussion

Figure 1a is the TEM image of the C-V_8C_7(rods), which shows the rods with the width of around 1 nm and length of several nanometers that are uniformly dispersed on carbon matrix. Figure 1b is the magnified TEM image of C-V_8C_7(rods), inset shows a rod with the width of 1.5 nm, length of 5.6 nm and lattice of V_8C_7 (222) facet. Figure 1c displays the corresponding width distribution of the rods. From randomly selected 100 rods, the average width of the rods was calculated as 0.8 nm, being angstrom scale. Figure 1d is the TEM image of C-V_8C_7(particles), which shows obvious agglomerations, due to the high concentration of SOV in the preparation step.

Figure 2 shows the XRD patterns of C-V_8C_7(particles) and C-V_8C_7(rods) (solid lines). The diffraction peaks at 2θ of 37.4°, 43.4°, 63.0° and 75.6° correspond to (222), (400), (440) and (622) facets of V_8C_7 crystal respectively, confirming that the rods and particles in Figure 1 are V_8C_7. The peak intensity of the V_8C_7 weakened with the decreasing concentration of SOV, which related to the V_8C_7 particle size.

The formation of V_8C_7 rods should be due to long-chain structure of the D201×1 resin. A proper concentration of SOV would lead to discontinuous chain of V_8C_7, i.e. V_8C_7 rods. However, a high concentration of SOV would lead to conglomerated chain, i. e. V_8C_7 particles.

The XRD patterns of Pt/C-V_8C_7(rods) and Pt/C-V_8C_7(particles) are also shown in Figure 2 (dotted lines). The peaks at 39.8°, 46.2° and 67.5° correspond to the (111), (200) and (220) facets of Pt crystal respectively. And the V_8C_7 peaks and the Pt peaks are overlapped with each other.

Figure 3 shows the TEM images of Pt/C-V_8C_7(rods) and Pt/C-V_8C_7(particles). Due

to that the C-V_8C_7 composites have different V_8C_7 content (leading to different density), Pt particles on C-V_8C_7(rods) are sparse (see Figure 3a), and on C-V_8C_7(particles) seem to be abundant (see Figure 3b). Inset of Figure 3a shows the EDS pattern of Pt/C-V_8C_7(rods) with C, Cu, V, Pt and Cr elements (Cu and Cr come from sample bracket). And Figure 3c shows the V_8C_7 (400) and Pt (111) lattices in Pt/C-V_8C_7(rods). They all prove the coexistence of V_8C_7 and Pt.

The MOR performances of the Pt/C-V_8C_7 electrocatalysts were tested and shown in Figure 4. Figure 4a shows the cyclic voltammograms of MOR on Pt/C-V_8C_7(rods), Pt/C-V_8C_7(particles) and commercial Pt/C electrocatalysts. It can be seen that the onset potential of these electrocatalysts is in the following order: Pt/C-V_8C_7(rods) (+0.25 V) < Pt/C-V_8C_7(particles) (+0.27 V) < commercial Pt/C (+0.39 V). The mass current densities are in the following order: Pt/C-V_8C_7(rods) (1605 mA mg_{Pt}^{-1}) > Pt/C-V_8C_7(particles) (1377 mA mg_{Pt}^{-1}) > commercial Pt/C (775 mA mg_{Pt}^{-1}). And the corresponding mass current density ratio is 2.07 : 1.78 : 1. Significantly, the onset potential for methanol oxidation on Pt/C-V_8C_7(rods) was negatively shifted for 140 mV compared with that on Pt/C. This is a great improvement since a direct methanol fuel cell gives only less than 0.5 V output at reasonable current density, leading to an expected 28% improvement in electric efficiency. Figure 4b shows the electrochemical active surface areas (EASAs) of the electrodes. The EASA is in the following order: Pt/C-V_8C_7(rods) (62.0 m^2g^{-1}) > Pt/C-V_8C_7(particles) (50.1 m^2g^{-1}) > commercial Pt/C (44.7 m^2g^{-1}). And the corresponding EASA ratio is 1.39 : 1.12 : 1. It can be seen that the mass current density ratio (2.07 : 1.78 : 1) is larger than the EASA

ratio (1.39 : 1.12 : 1), that is to say, the EASA is not the sole factor to determine the catalytic performances. By comparing the ingredients of Pt/C-V_8C_7 and Pt/C, it can be deduced that the other factor to increase the catalytic activity of Pt/C-V_8C_7 should be the promotion effect of V_8C_7 on Pt. As to the higher activity of Pt/C-V_8C_7(rods) than that of Pt/C-V_8C_7(particles), it is related to the smaller size of V_8C_7 rods, which have higher specific surface area or more sites to interact with the Pt particles. Significantly, it is very energy-efficient that the Pt/C-V_8C_7(rods) has only one-tenth V_8C_7 content that of the Pt/C-V_8C_7(particles). More significantly, the enhancement of the current densities at lower potentials was much higher as shown in Figure 4c, showing that the ratio of the current density on Pt/C-V_8C_7(rods) over the current density on Pt/C exceeds 9 at 0.4 V.

The stabilities of the Pt/C-V_8C_7(rods) and Pt/C electrodes for MOR are shown in Figure 5. The shadows in Figure 5 are the cycling difference between the 1st cycle and the 2,000th cycle. It is clear that the activity of the commercial Pt/C reduced 27.7% from 775 mA mg_{Pt}^{-1} to 560 mA mg_{Pt}^{-1} for MOR by comparing the peak current density. However, the activity of the Pt/C-V_8C_7(rods) reduced 9.4 % from 1605 mA mg_{Pt}^{-1} to 1470 mA mg_{Pt}^{-1}. The results indicate that the Pt/C-V_8C_7(rods) electrocatalyst is more stable than the commercial Pt/C.

Literature reported that electron transfer (synergistic effect) exists between carbides and the loaded noble metals, which not only improves the oxidation of methanol and the intermediate poisons due to easy electron-transfer,[1] but also increases the stability due to increased linkage strength between carbides and noble metals.[24] The

synergistic effect may account for the promotion effect of V_8C_7 on the excellent activity and stability of the Pt/C-V_8C_7(rods) electrocatalyst.

4. Conclusions

Angstrom-scale V_8C_7 rods have been successfully synthesized through an ion-exchange route. The angstrom-scale C-V_8C_7(rods) show higher promotion effect than nanoscale C-V_8C_7(particles) on the performance of Pt electrocatalysts, although the former has only one-tenth V_8C_7 content that of the latter. Moreover, the Pt/C-V_8C_7(rods) electrocatalyst shows much higher activity and stability than the commercial Pt/C for MOR.

Acknowledgements

This work was funded by National Natural Science Foundations of China (21306067), China Postdoctoral Science Foundation (2014T70481), Natural Science Foundation of Jiangsu (BK20130490, BK20140531), Industry High Technology Foundation of Jiangsu (BE2013090) and Zhenjiang Industry Supporting Plan (GY2013023).

References

1 G. Cui, P. K. Shen, H. Meng, J. Zhao and G. Wu, *J. Power Sources*, 2011, **196**, 6125-6130.

2 H. Meng and P. K. Shen, *Chem. Commun.,* 2005, 4408-4410.

3 Z. Zhao, X. Fang, Y. Li, Y. Wang, P. K. Shen, F. Xie and X. Zhang, *Electrochem. Commun.,* 2009, **11**, 290-293.

4 Y. W. Lee, A. R. Ko, D. Y. Kim, S. B. Han and K. W. Park, *RSC Adv.*, 2012, **2**, 1119-1125.

5 Y. Dong, H. Pang, H. Yang, J. Jiang, Y. Chi and T. Yu, *RSC Adv.*, 2014, **4**, 32791-32795.

6 C. W. Liu, C. M. Lai, J. N. Lin, L. D. Tsai and K. W. Wang, *RSC Adv.*, 2014, **4**, 15820-15824.

7 S. Sepp, E. Härk, P. Valk, K. Vaarmets, J. Nerut, R. Jäger and E. Lust, *J. Solid State Electr.,* 2014, **18**, 1223-1229.

8 M. Shi, L. Kang, Y. Jiang and C. Ma, *Catal. Lett.,* 2014, **144**, 278-284.

9 C. Liang, L. Ding, C. Li, M. Pang, D. Su, W. Li and Y. Wang, *Energ. Environ. Sci.,* 2010, **3**, 1121-1127.

10 Y. W. Lee, A. R. Ko, S. B. Han, H. S. Kim, D. Y. Kim, S. J. Kim and K. W. Park, *Chem. Commun.,* 2010, **46**, 9241-9243.

11 C. Ma, W. Liu, M. Shi, X. Lang, Y. Chu, Z. Chen, D. Zhao, W. Lin and C. Hardacre, *Electrochim. Acta,* 2013, **114**, 133-141.

12 J. L. Lu, Z. H. Li, S. P. Jiang, P. K. Shen and L. Li, *J. Power Sources,* 2012, **202**, 56-62.

13 Z. Yan, M. Cai and P. K. Shen, *Sci. Rep.-Uk,* 2013, **3**, 1646.

14 Z. Yan, G. He, M. Cai, H. Meng and P. K. Shen, *J. Power Sources,* 2013, **242**, 817-823.

15 Y. J. Wang, D. P. Wilkinson and J. Zhang, *Chem. Rev.,* 2011, **111**, 7625-7651.

16 R. Ganesan and J. S. Lee, *Angew. Chem. Int. Edit.,* 2005, **44**, 6557-6560.

17 J. Yang, Y. Xie, R. Wang, B. Jiang, C. Tian, G. Mu, J. Yin, B. Wang and H. Fu, *Acs. Appl. Mater. Inter.,* 2013, **5**, 6571−6579.

18 Z. J. Mellinger, T. G. Kelly and J. G. Chen, *ACS Catal.,* 2012, **2**, 751−758.

19 C. Xu, M. Shi, L. Kang and C. Ma, *Mater. Lett.,* 2013, **91**, 183-186.

20 Q. Zhu, S. Zhou, X. Wang and S. Dai, *J. Power Sources,* 2009, **193**, 495-500.

21 I. J. Hsua, Y. C. Kimmela, Y. Dai, S. Chen and J. G. Chen, *J. Power Sources,* 2012, **199**, 46-52.

22 M. Yin, Q. Li, J. O. Jensen, Y. Huang, L. N. Cleemann, N. J. Bjerrum and W. Xing, *J. Power Sources,* 2012, **219**, 106-111.

23 X. B. Gong, S. J. You, X. H. Wang, Y. Gan, R. N. Zhang and N. Q. Ren, *J. Power Sources,* 2013, **225**, 330-337.

24 Z. Yan, G. He, P. K. Shen, Z. Luo, J. Xie and M. Chen, *J. Mater. Chem. A,* 2014, **2**, 4014-4022.

25 Z. Yan, J. Xie, P. K. Shen, M. Zhang, Y. Zhang and M. Chen, *Electrochim. Acta,* 2013, **108**, 644-650.

26 K. G. Nishanth, P. Sridhar, S. Pitchumani and A. K. Shukla, *Fuel Cells*, 2012, **12**, 146-152.

27 O. Guillén-Villafuerte, G. García, J. L. Rodsríguez, E. Pastor, R. Guil-López, E. Nieto and J. L. G. Fierro, *Int. J. Hydrogen Energy,* 2013, **38**, 7811-7821.

28 Z. Yan, H. Wang, M. Zhang, Z. Jiang, T. Jiang and J. Xie, *Electrochim. Acta,* 2013, **95**, 218-224.

29 G. He, Z. Yan, X. Ma, H. Meng, P. K. Shen and C. Wang, *Nanoscale,* 2011, **3**, 3578-3582.

30 B. Zhang and Z. Q. Li, *J. Alloy. Compd.,* 2005, **392**, 183-186.

31 Z. W. Zhao, H. S. Zuo, Y. Liu, W. Q. Song, S. F. Mao and Y. R. Wang, *Int. J. Refract. Met. H.,* 2009, **27**, 971-975.

32 Z. Yan, M. Zhang, J. Xie and P. K. Shen, *J. Power Sources,* 2013, **243**, 336-342.

33 Z. Hu, C. Chen, H. Meng, R. Wang, P. K. Shen and H. Fu, *Electrochem. Commun.,* 2011, **13**, 763-765.

34 Z. Yan, M. Cai and P. K. Shen, *J. Mater. Chem.,* 2011, **21**, 19166-19170.

35 G. He, Z. Yan, M. Cai, P. K. Shen, M. R. Gao, H. B. Yao and S. H. Yu, *Chem.-Eur. J.,* 2012, **18**, 8490-8497.

36 Z. Q. Tian, S. P. Jiang, Y. M. Liang and P. K. Shen, *J. Phys. Chem. B,* 2006, **110**, 5343-5350.

Figure Captions

Figure 1 (a) TEM and (b) magnified TEM images of C-V_8C_7(rods); (c) rods' width distribution of V_8C_7(rods); (d) TEM image of C-V_8C_7(particles). Inset of (b) is the TEM image of a V_8C_7 rod.

Figure 2 XRD patterns of C-V_8C_7(rods), C-V_8C_7(particles), Pt/C-V_8C_7(rods) and Pt/C-V_8C_7(particles).

Figure 3 TEM images of (a) Pt/C-V_8C_7(rods) and (b) Pt/C-V_8C_7(particles); (c) HRTEM image of Pt/C-V_8C_7(rods). Inset of (a) is the corresponding EDS pattern.

Figure 4 The cyclic voltammograms on Pt/C-V_8C_7(rods), Pt/C-V_8C_7(particles) and Pt/C electrocatalysts in (a) 0.5 mol L^{-1} H_2SO_4/1.0 mol L^{-1} methanol solution and (b) 0.5 mol L^{-1} H_2SO_4 solution, with the scan rate of 50 mV s^{-1} at 30 ^oC; (c) the plot of the ratio of the current density on Pt/C-V_8C_7(rods) to that on Pt/C.

Figure 5 The cyclic voltammograms on Pt/C-V_8C_7(rods) and Pt/C electrodes in (a) 0.5 mol L^{-1} H_2SO_4/1.0 mol L^{-1} methanol solution and (b) 0.5 mol L^{-1} H_2SO_4 solution, with the scan rate of 50 mV s^{-1} at 30 ^oC. The shadows show the difference between the 1^{st} cycle and the $2{,}000^{th}$ cycle.

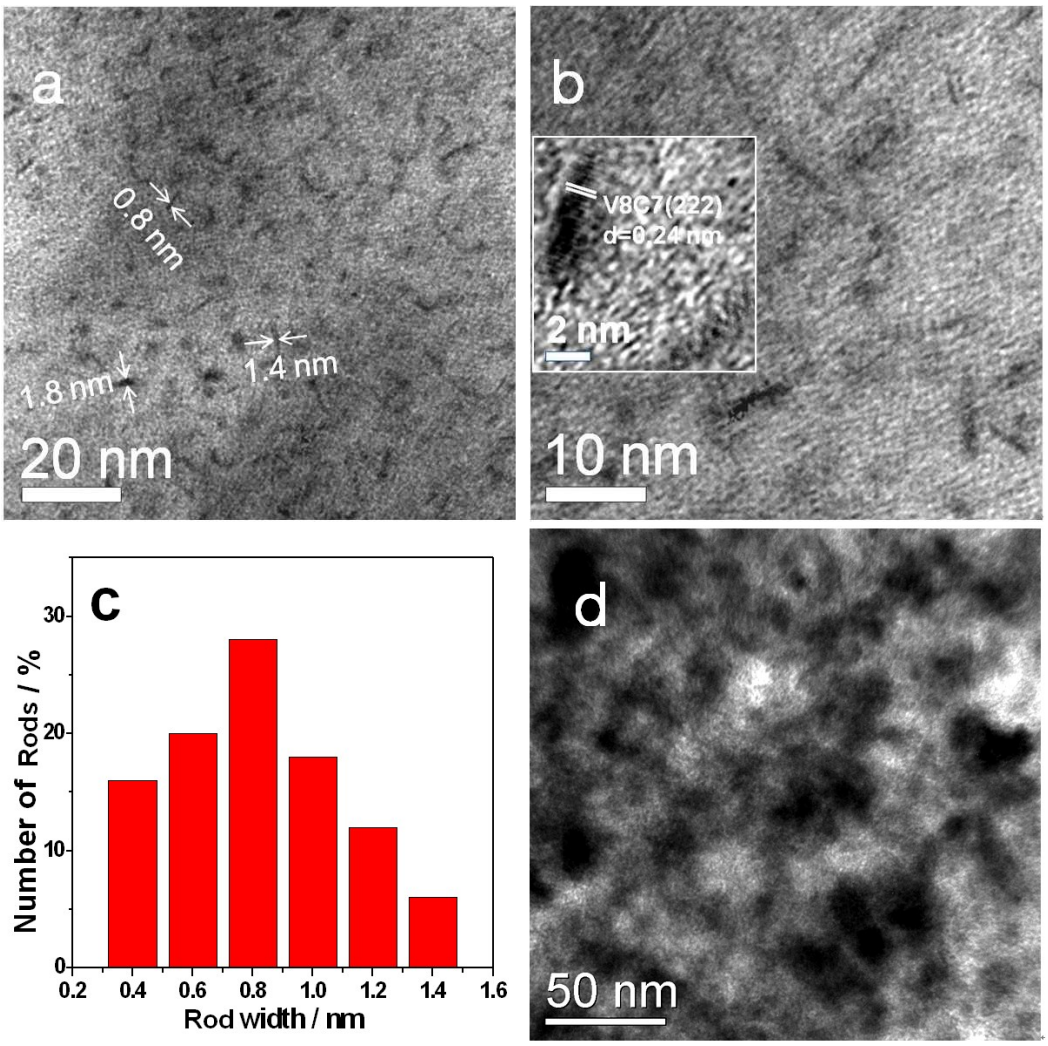

Figure 1

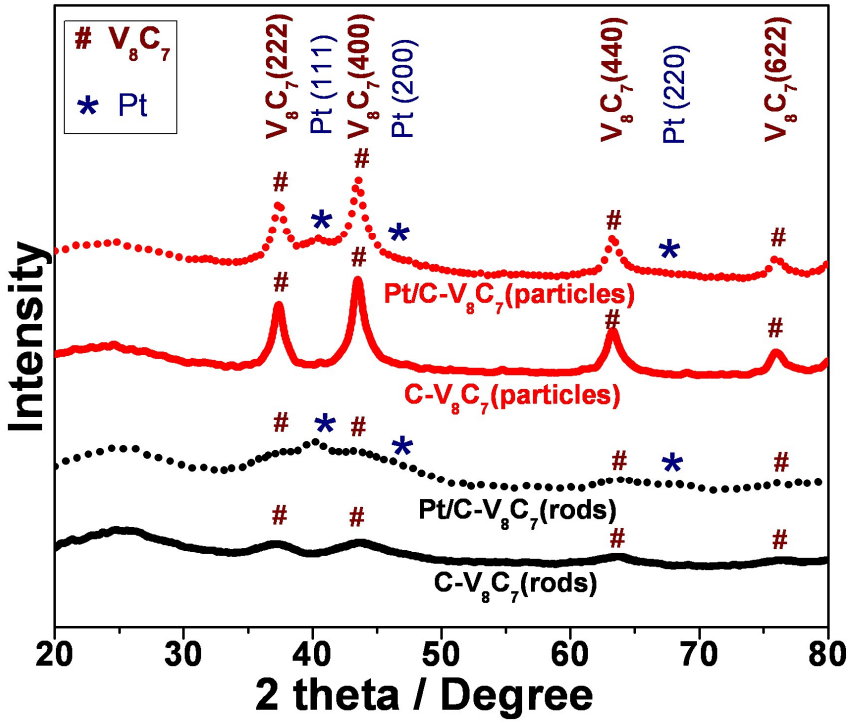

Figure 2

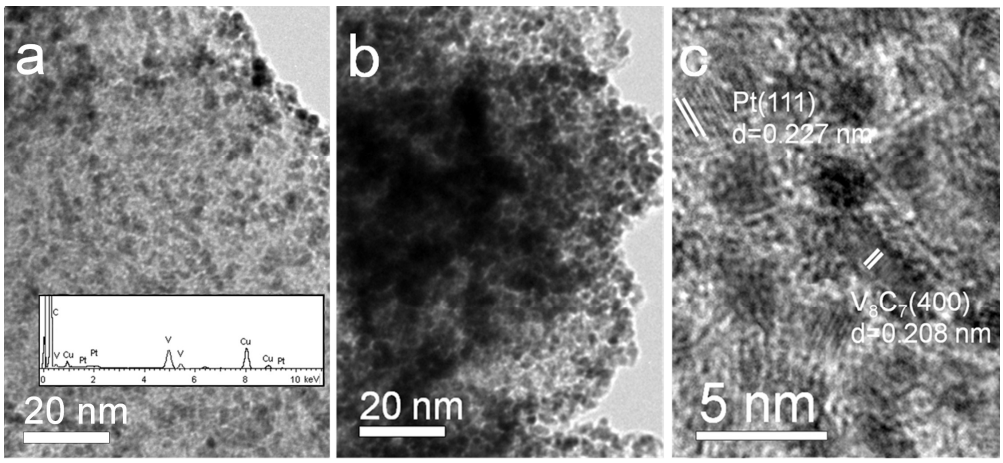

Figure 3

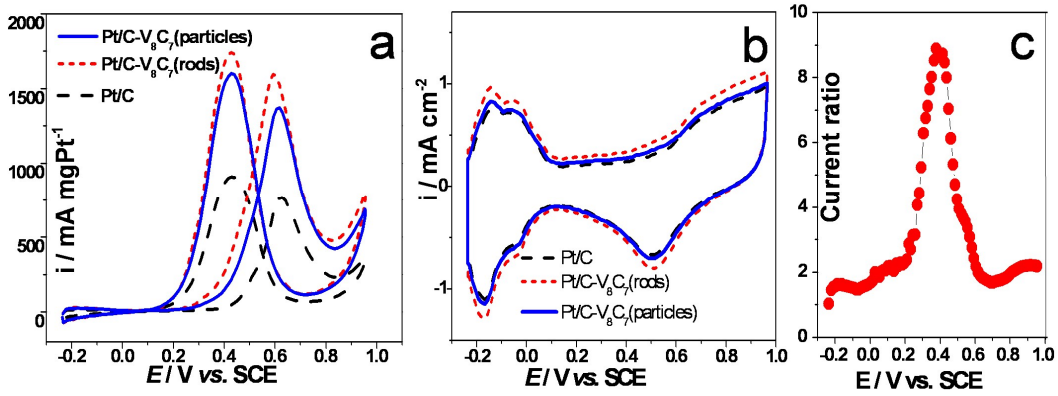

Figure 4

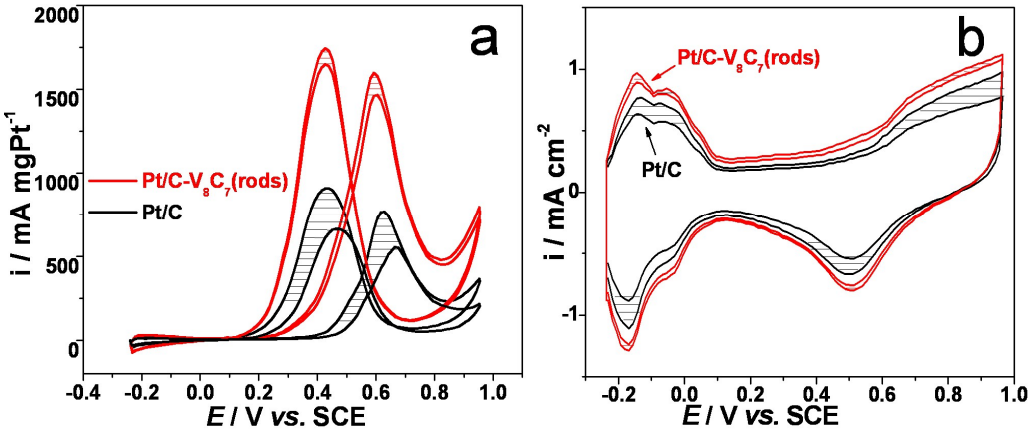

Figure 5